ISOTOPE SPECIFIC Zn(n,p)Cu ACTIVATION MODELING IN ZnO NANOPARTICLES UNDER FAST NEUTRON SPECTRA

ILAHA V. IZZATOVA
Institute of Radiation Problems of Ministry of Science and Education AZ1143, B.Vahabzade 9, Baku, Azerbaijan

Zinc oxide (ZnO) nanoparticles are increasingly used in neutron fields, where zinc activation and copper buildup affect both safety and functional performance. This article presents an isotope resolved modeling study of Zn(n,p)Cu activation in ZnO nanoparticles based on harmonized excitation functions for the ^{64}Zn(n,p)^{64}Cu, ^{66}Zn(n,p)^{66}Cu, ^{67}Zn(n,p)^{67}Cu and ^{68}Zn(n,p)^{68}Cu reactions. Cross sections calculated with the computer code are mapped onto a common 0–20 MeV energy grid, folded with representative fast neutron spectra and coupled to Bateman inventory calculations for natural zinc in ZnO. The results reveal a clear hierarchy, with ^{64}Zn(n,p)^{64}Cu dominating the fast spectrum response, ^{68}Zn(n,p)^{68}Cu providing a secondary contribution and ^{66}Zn(n,p)^{66}Cu remaining minor. Despite its low cross section, ^{67}Zn(n,p)^{67}Cu generates medium lived ^{67}Cu that governs the residual copper inventory. The framework provides a compact basis for predicting activation in ZnO based components and for optimizing irradiation conditions for tailored copper production.

Keywords: ZnO nanoparticles; zinc activation; Zn(n,p)Cu reactions; copper radionuclides.
DOI:10.70784/azip.1.2025424

1. INTRODUCTION

Zinc oxide (ZnO) nanoparticles are widely deployed in electronics, optics, sensing and catalysis, where their large surface-to-volume ratio, tunable band structure and defect chemistry offer significant performance advantages over bulk ZnO [1-6]. In many of these applications, ZnO-based devices or coatings operate in mixed neutron–photon fields, for example in research reactors, spallation sources, shielding and detector assemblies, or in high-flux test environments designed for materials qualification. Under such conditions, neutron-induced activation of zinc isotopes becomes a key factor for both radiological safety and functional performance [7-11].

Natural zinc is composed of several stable isotopes (^{64}Zn, ^{66}Zn, ^{67}Zn and ^{68}Zn), which open different reaction channels under fast-neutron irradiation. Of particular interest are (n,p) reactions producing copper radionuclides ^{64}Cu, ^{66}Cu, ^{67}Cu and ^{68}Cu. These radionuclides contribute to the activation inventory of ZnO nanomaterials, but they can also be exploited functionally. Among them, ^{67}Cu is especially attractive as a medium-lived isotope suitable for post-irradiation diagnostics and as a potential tracer, provided that its buildup can be predicted with sufficient accuracy as a function of spectrum, fluence and initial isotopic composition.

The design and deployment of ZnO nanoparticle systems in neutron fields therefore requires isotope-resolved excitation functions for Zn(n,p)→Cu reactions over the relevant fast-energy range. Conventional evaluations and databases provide reaction cross sections, but often with heterogeneous formats, energy grids or normalization, complicating one-to-one comparison across isotopes. Moreover, most activation benchmarks have been developed for bulk or macroscopic geometries, whereas nanoparticles exhibit strongly reduced self-shielding and distinct recoil-transport behavior, leading to different spatial distributions of reaction products and defects.

Recent work has highlighted how neutron transmutation can be used as a tool to control the physical properties of nanomaterials at the atomic scale, for example by tailoring dopant concentrations in carbides and oxides or modulating conductivity in neutron-irradiated β-SiC through trace and dopant elements [12-18]. Building on these concepts, ZnO nanoparticle systems irradiated in research reactors or test facilities are attractive candidates for controlled generation of copper isotopes within a robust oxide host [19-22]. In this context, ^{67}Zn(n,p)^{67}Cu provides a strategically important, though relatively weak, channel for medium-lived ^{67}Cu production. The present work compiles and analyzes isotope-resolved excitation functions for ^{64}Zn(n,p)^{64}Cu, ^{66}Zn(n,p)^{66}Cu, ^{67}Zn(n,p)^{67}Cu and ^{68}Zn(n,p)^{68}Cu on a harmonized energy–cross-section grid tailored to ZnO nanoparticle applications. Using computer simulation outputs formatted as Incident Energy (MeV) versus Cross Section (barns), we present a coherent set of excitation functions suitable for direct spectrum folding and inventory modeling. All curves are presented on consistent axes, enabling like-for-like comparison across isotopes and clearly revealing threshold-dominated behavior, magnitude differences and relative contributions to copper inventories in fast spectra.

Special attention is given to the ^{67}Zn(n,p)^{67}Cu reaction, whose cross section is small but non-negligible when integrated over realistic spectra, and whose product ^{67}Cu sustains a medium-lived post-irradiation source term. We also discuss how nanoscale geometry affects self-shielding, proton emission and recoil ranges, and what this implies for defect distributions and the retention or loss of reaction products in ZnO nanoparticle powders and coatings. The resulting excitation functions and inventory trends provide a compact, decision-ready basis for forecasting isotope-resolved copper buildup

131, H.Javid ave, AZ-1073, Baku
Institute of Physics
E-mail: jophphysics@gmail.com

in ZnO nanomaterials under fast-neutron exposure and for tailoring irradiation conditions when ^{67}Cu yield or activation control is a priority.

2. CROSS-SECTION DATA AND PROCESSING

To evaluate zinc (n,p) activation in ZnO nanoparticles, we consider representative fast-neutron spectra typical of materials-testing positions in research reactors and other mixed-field facilities. For each spectrum, the neutron flux $\varphi(E)$ is discretized on a fine energy grid spanning 0–20 MeV with increased resolution in the threshold region where (n,p) channels open and rise. The same incident-energy grid is used for all zinc isotopes, ensuring that the resulting excitation functions $\sigma_i(E)$ can be compared directly and folded consistently with arbitrary spectra. In practice, the energy mesh is chosen to be sufficiently dense to resolve the onset and peak structures of the (n,p) cross sections, while keeping the computational cost of inventory calculations moderate.

Isotope-resolved excitation functions for ^{64}Zn(n,p)^{64}Cu, ^{66}Zn(n,p)^{66}Cu, ^{67}Zn(n,p)^{67}Cu and ^{68}Zn(n,p)^{68}Cu are obtained from evaluated nuclear data libraries and/or reaction-model calculations (NNDS). For each reaction, the pointwise cross section $\sigma(E)$ is interpolated onto the common energy grid described above. To facilitate direct graphical comparison, the excitation functions are plotted with harmonized axes and Incident Energy (MeV), spanning 0–20 MeV for all isotopes. Cross Section (barns), using linear or logarithmic scales as appropriate to cover the relevant magnitude range for each reaction channel. For ^{64}Zn(n,p)^{64}Cu and ^{68}Zn(n,p)^{68}Cu, linear-scaled panels highlight peak cross sections up to ~10^{-1}–$10^{-0.2}$ b and ~3×10^{-2} b, respectively. For the weaker ^{66}Zn(n,p)^{66}Cu and ^{67}Zn(n,p)^{67}Cu channels, logarithmic ordinates are employed, with ranges from 10^{-6} to 10^{-2} b for ^{66}Zn and from 10^{-10} to 10^{-1} b for ^{67}Zn, emphasizing both low-probability tails and threshold-driven rise.

3. RESULT AND DISCUSSION

The starting point of our analysis is the ^{64}Zn(n,p)^{64}Cu excitation function, which defines the strongest (n,p) channel in natural zinc and therefore sets the upper bound for copper activation in ZnO-based systems. As shown in Fig. 1, the reaction exhibits a typical threshold-type behavior: the cross section is negligible at low neutron energies, rises steeply once the threshold region is reached, and then evolves into a broad maximum in the fast-energy range. This confirms that ^{64}Zn(n,p)^{64}Cu is effectively a fast-spectrum reaction, with copper production controlled almost entirely by the high-energy tail of the neutron flux rather than by thermal or epithermal neutrons. When this excitation function is folded with representative research-reactor spectra, ^{64}Zn emerges as the dominant contributor to the short-lived copper inventory during and immediately after irradiation, providing a natural reference against which the weaker ^{66}Zn, ^{67}Zn and ^{68}Zn (n,p) channels can be interpreted in the following sections.

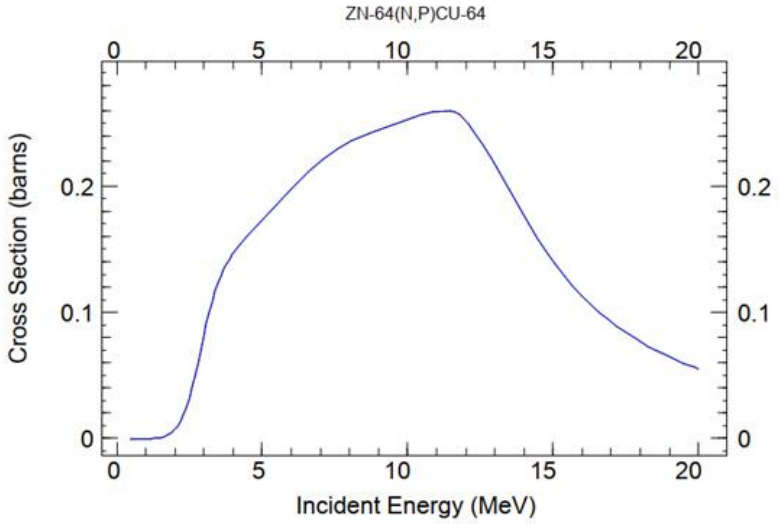

Fig. 1. Excitation function of the ^{64}Zn(n,p)^{64}Cu reaction.

In contrast, the ^{66}Zn(n,p)^{66}Cu excitation function in Fig. 2 highlights the behavior of a much weaker (n,p) channel. The cross section remains confined to the 10^{-6}–10^{-2} barn range across 0–20 MeV, several orders of magnitude below the ^{64}Zn(n,p)^{64}Cu response. Although the same threshold-controlled increase is observed in the fast-energy region, spectrum folding demonstrates that ^{66}Zn contributes only marginally to the overall copper inventory in natural ZnO. Consequently, ^{66}Cu can be treated as a minor correction term in activation and radiological assessments, while still being explicitly tracked in inventory calculations for completeness and for benchmarking reaction-model predictions in the weak-channel limit.

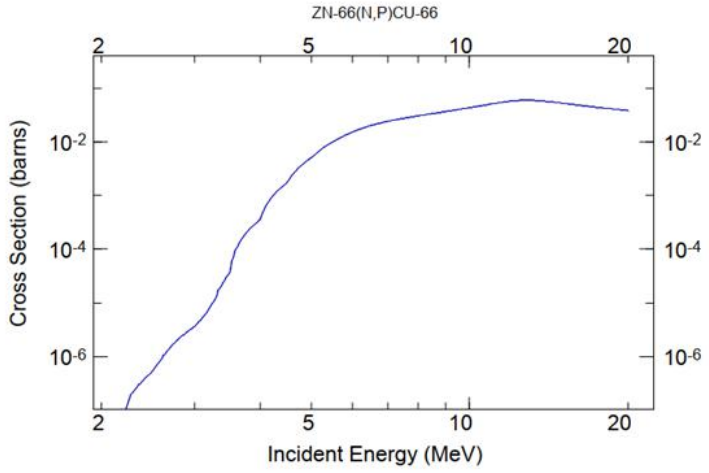

Fig. 2. Excitation function of the $^{66}Zn(n,p)^{66}Cu$ reaction.

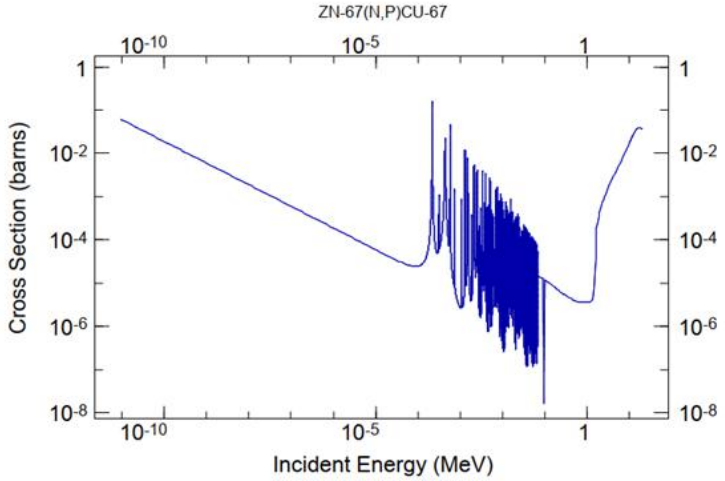

Fig. 3. Excitation function of the $^{67}Zn(n,p)^{67}Cu$ reaction.

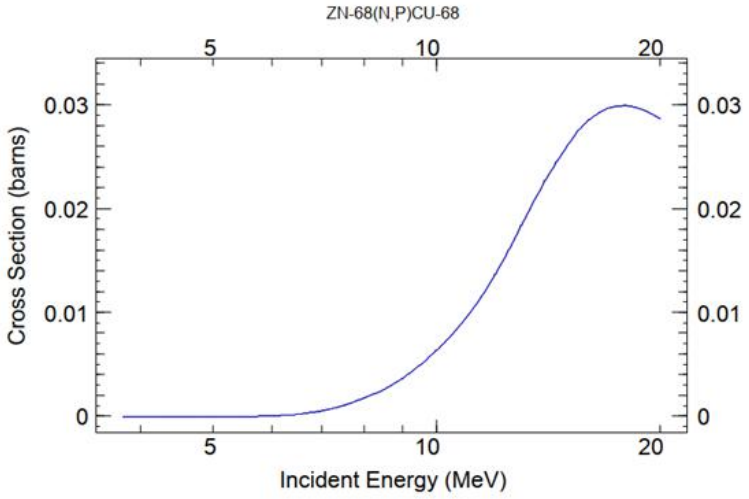

Fig. 4. Excitation function of the $^{68}Zn(n,p)^{68}Cu$ reaction.

The $^{67}Zn(n,p)^{67}Cu$ excitation function in Fig. 3 further illustrates the behavior of an intrinsically weak but strategically important (n,p) channel. On double-logarithmic axes, the cross section remains small across the entire energy range, confirming that ^{67}Zn makes only a minor contribution to the instantaneous (on-beam) copper activity in natural ZnO. However, when folded with representative fast-neutron spectra

and propagated through the inventory calculations, even this low cross section leads to a finite ^{67}Cu buildup at high fluence. Given the medium-lived character of ^{67}Cu, the ^{67}Zn(n,p)^{67}Cu reaction becomes a key source of residual activity during the post-irradiation period and a potential handle for using ZnO nanoparticles as activation-based probes of neutron field characteristics.

The excitation function for ^{68}Zn(n,p)^{68}Cu in Fig. 4 represents an intermediate case between the dominant ^{64}Zn channel and the weak ^{66}Zn and ^{67}Zn reactions. The cross section remains strictly threshold-controlled, but attains peak values of only a few $\times 10^{-2}$ barn in the fast-energy range. When folded with representative reactor spectra and weighted by the natural abundance of ^{68}Zn, this still yields a noticeable contribution to the total copper inventory in ZnO, particularly during irradiation and early cooldown when ^{68}Cu is present together with ^{64}Cu. In practical activation assessments, ^{68}Zn(n,p)^{68}Cu therefore acts as a secondary but non-negligible source term, and its excitation function provides an important complement to the ^{64}Zn-based reference when modeling isotope-resolved copper buildup in ZnO nanoparticle systems.

Bringing these trends together, the four excitation functions establish a clear, isotope-resolved hierarchy for Zn(n,p)→Cu activation in ZnO nanoparticle systems. The ^{64}Zn(n,p)^{64}Cu channel (Fig. 1) dominates the fast-spectrum response and controls the short-term copper activity, with ^{68}Zn(n,p)^{68}Cu (Fig. 4) providing a secondary but non-negligible contribution during irradiation and early cooldown. In contrast, the ^{66}Zn(n,p)^{66}Cu reaction (Fig. 2) remains a minor correction across all energies, while ^{67}Zn(n,p)^{67}Cu (Fig. 3) represents a weak but strategically important path to medium-lived ^{67}Cu, which governs the residual copper inventory at longer times. In the nanoparticle regime, reduced self-shielding ensures that these isotope-specific excitation functions translate directly into spectrum-averaged cross sections and time-dependent inventories, making ZnO nanoparticles an efficient platform for both activation management and tailored ^{67}Cu generation in neutron-irradiation environments.

4. CONCLUSIONS

In this work, developed an isotope-resolved description of Zn(n,p)→Cu activation in ZnO nanoparticle systems by compiling and analyzing excitation functions for the ^{64}Zn(n,p)^{64}Cu, ^{66}Zn(n,p)^{66}Cu, ^{67}Zn(n,p)^{67}Cu and ^{68}Zn(n,p)^{68}Cu reactions on a common energy grid. All curves were presented on harmonized axes (incident energy in MeV, cross section in barns), enabling direct comparison of threshold behavior, peak magnitudes and overall shapes across the zinc isotopes. These excitation functions were then folded with representative fast-neutron spectra and used as input to activation–inventory calculations tailored to ZnO nanoparticle geometries. The results establish a clear hierarchy of (n,p) channels in natural zinc. The ^{64}Zn(n,p)^{64}Cu reaction is the dominant contributor to copper activation, with ^{68}Zn(n,p)^{68}Cu providing a secondary but still significant contribution during irradiation and early cooldown. In contrast, ^{66}Zn(n,p)^{66}Cu remains a weak channel that can usually be treated as a minor correction in radiological assessments. The ^{67}Zn(n,p)^{67}Cu reaction is also intrinsically weak in terms of cross section, but it yields the medium-lived radionuclide ^{67}Cu, which becomes strategically important for the residual copper inventory at longer times and for potential diagnostic or tracer applications.

In the nanoparticle regime, strongly reduced self-shielding means that these isotope-specific excitation functions map efficiently onto spectrum-averaged cross sections and time-dependent inventories in ZnO. This makes ZnO nanoparticles attractive both as functional materials and as activation probes in mixed neutron fields, where the combined ^{64}Cu–^{68}Cu short-term response and ^{67}Cu medium-term signal encode key features of the fast spectrum and fluence history. Future work should couple these modeling frameworks with gamma-spectroscopic activation measurements and microstructural characterization of irradiated ZnO nanoparticles, closing the loop between reaction physics, defect evolution and functional property changes.

[1] *Benjian Liu* et al. "Enhanced performance of diamond Schottky nuclear batteries by using ZnO as electron transport layer" Diamond and Related Materials 109, 2020, 108026

[2] *Xuan Lai* et al. "ZnO NPs delay the recovery of psoriasis-like skin lesions through promoting nuclear translocation of p-NFκB p65 and cysteine deficiency in keratinocytes" Journal of Hazardous Materials 410, 2021, 124566

[3] *Buse Ozen Ilik* et al. "Elucidating the influences of Tantalum (V) oxide in Bi_2O_3–TeO_2–ZnO ternary glasses: An experimental characterization study on optical and nuclear radiation transmission properties of high-density glasses" Ceramics International 49, 2023, 10906-10913

[4] *R. El-Mallawany* et al. "Optical properties and nuclear radiation shielding capacity of TeO_2-Li_2O-ZnO glasses" Optical Materials 106, 2020, 109988

[5] *Y.S. Rammah* et al. "Role of ZnO on TeO_2.Li_2O.ZnO glasses for optical and nuclear radiation shielding applications utilizing MCNP5 simulations and WINXCOM program" Journal of Non-Crystalline Solids 544, 2020, 120162

[6] *A.S. Abouhaswa* et al. "Nuclear shielding properties of B_2O_3–Pb_3O_4–ZnO glasses: Multiple impacts of Er_2O_3 additive" Ceramics International 46, 2020, 27849-27859

[7] *M.I. Sayyed* et al. "Tuning structural, optical, and radiation shielding properties of ZnO-enriched B_2O_3-Na_2O-CaO-Y_2O_3-La_2O_3 borate

glasses" Journal of Alloys and Compounds 1044, 2025, 184478

[8] *M. Kh. Hamad*. "Optical, photon interaction, and radiation shielding performance of Ho_2O_3-doped borate glasses modified with ZnO and CaO" Materials Research Bulletin 194, 2026, 113785

[9] *M.H.A. Mhareb* et al. "The correlation between optical, mechanical, and radiation shielding properties for SiO_2–ZnO–PbO_2 glass samples doped with different concentrations of Gd_2O_3" Radiation Physics and Chemistry 239, 2026, 113325

[10] *M.I. Sayyed* et al. "Revealing optical, mechanical and radiation shielding behavior of ZnO-PbO_2-SiO_2 Glasses" Chemical Physics Impact 11, 2025, 100949

[11] *Flávio Henrique Covolam Boldrin* et al. "The effect of calcination temperature on the performance of the CX/ZnO-Cu_xO in sulfamerazine photodegradation under solar and visible radiation" Optical Materials 168, 2025, 117404

[12] *Elchin M. Huseynov, Anze Jazbec* "Application of neutron transmutation technology to control the physical properties of nanoparticles at the atomic scale" Carbon 229, 119568, 2024

[13] *Elchin M. Huseynov*. "Modulation of conductivity in neutron-irradiated nanocrystalline β-SiC through trace and dopant elements" Journal of Electronic Materials 54, 2025, 8920–8934

[14] *Elchin M. Huseynov*. "FTIR spectroscopy of ZrC nanoparticles under the gamma radiation" Spectrochimica Acta Part A: Molecular and Biomolecular Spectroscopy 286, 122032, 2023

[15] *Elchin M. Huseynov, Tural G. Naghiyev, Nijat R. Abbasov*. "The paramagnetic approach of the color-changing of nano h-BN particle under the neutron irradiation" Physica E: Low-dimensional Systems and Nanostructures 139, 115124, 2022

[16] *Elchin M. Huseynov, Tural G. Naghiyev*. "Various thermal parameters investigation of 3C-SiC nanoparticles at the different heating rates" Applied Physics A 128, 115, 2022,

[17] *Elchin M. Huseynov, Jale G. Atakishiyeva*. "Characterizing neutron irradiation-induced effects in the nanocrystalline B_4C particles using EPR spectroscopy" Solid State Sciences 154, 107604, 2024

[18] *Elchin M. Huseynov, Tural G. Naghiyev*. "Low temperature DSC investigation of neutron irradiated non-crystalline Si_3N_4 nanoparticles" Journal of Non-Crystalline Solids 647, 2025, 123272

[19] *Abely E. Mwakuna* et al. "ZnO-modified magnesium lead borate glasses: Optical, mechanical, and radiation shielding characteristics" Journal of Radiation Research and Applied Sciences 18, 2025, 101827

[20] *M.I. Sayyed* et al. "Enhancement of the radiation shielding properties of lead-borate glass: the impacts of Sb_2O_3, Al_2O_3 and ZnO" Radiation Physics and Chemistry 237, 2025, 113109

[21] *Aljawhara H. Almuqrin* et al. "Size matters: Radiation shielding superiority of borate glasses with nano vs. micro ZnO" Nuclear Engineering and Technology 57, 2025, 103614

[22] *Olubusayo F. Oladejo* et al. "Band engineering in ZnO/MoO_3 heterojunction photodetector for improved photoelectrical response toward highly rated ultraviolet radiation sensing" Physica B: Condensed Matter 706, 2025, 417155

Received: 17.11.2025